Creation of aspheric interfaces on an electrowetting liquid lens using surface oscillations

Strauch, Matthias; Somers, Peter; Bociort, Florian; Urbach, Paul

DOI
10.1063/1.5063994

Publication date
2018

Document Version
Final published version

Published in
AIP Advances

Creation of aspheric interfaces on an electrowetting liquid lens using surface oscillations

Matthias Strauch, Peter A. A. M. Somers, Florian Bociort, and H. Paul Urbach

Citation: AIP Advances **8**, 115224 (2018); doi: 10.1063/1.5063994
View online: https://doi.org/10.1063/1.5063994
View Table of Contents: http://aip.scitation.org/toc/adv/8/11
Published by the American Institute of Physics

Creation of aspheric interfaces on an electrowetting liquid lens using surface oscillations

Matthias Strauch,[a] Peter A. A. M. Somers, Florian Bociort, and H. Paul Urbach
Delft University of Technology, 2628CH Delft, The Netherlands

(Received 3 October 2018; accepted 15 November 2018; published online 27 November 2018)

A technique to create aspheric surface shapes on commercially available electrowetting liquid lenses is demonstrated. Based on a previously published surface oscillation model a technique using a Hankel transform is proposed and tested experimentally. An alternating actuation voltage is applied to the liquid lens to stimulate surface oscillations, that temporarily add up to the desired surface shape. The voltage signal can be repeated at video rate. The measurements were taken with a Mach-Zehnder interferometer and confirm the previous results. The capabilities and limitations of the proposed method are demonstrated using the examples of a Bessel surface, spherical aberration, an axicon, and a top hat structure.
https://doi.org/10.1063/1.5063994

I. INTRODUCTION

The performance of electrowetting liquid lenses is limited by surface oscillations. Already when the first liquid lenses (LL) were developed, it became clear, when switching the focal distance too fast, the liquids inertia prevents the liquid surface from following the change instantaneously.[1,2] Surface waves are created. These uncontrolled deviations from a spherical interface were identified as the cause of dynamic aberrations and have limited the operational speed of liquid lenses. All liquid lenses therefore have a response time, which depends on the chosen materials and the lens size, that limits their high-speed application.

Recent work shifted the focus towards this problem by optimizing the liquids and mechanical surfaces to minimize the response time.[3] But also static aberrations, especially spherical aberration, limit the performance in some applications[4] and in consequence, many new lenses have been developed to create aspheric liquid lenses, e.g., an ultrasonic liquid crystal lens[5] and a LL making use of thermal Marangoni forces[6] to shape its surface. Also, the combination of hydrostatic pressure and electrowetting or the use of multiple liquid interfaces promises to extend the functionality of a liquid lens.[7–10] However, only the simple electrowetting LL has been commercialized.

As an alternative approach we focused on studying the nature of surface waves on a commercially available liquid lens and its resonance modes in order to avoid, or even to make use of them.[11] By exciting the liquid interface faster than the response time of the LL, waves can be created on purpose to create new optical surface shapes. The resonant modes have the shape of Bessel functions and can be excited individually. A similar approach focusing on the application of surface waves on a liquid lens for optical encryption came to the same conclusion.[12] Surface oscillations of liquid droplets have been studied thoroughly elsewhere,[13,14] providing a good overview of liquid immersion and viscosity effects,[15,16] that are necessary to understand the non-linearity of the liquid oscillations.[17] However, a linear dispersion relation based on an inviscid and incompressible model of the liquid[18,19] was confirmed experimentally for small surface excitations up to a few optical path lengths. For a larger surface excitation instead, a deviation was detected that is similar to the dynamic response observed

[a]Electronic mail: m.strauch@tudelft.nl

in larger liquid lenses.[20] The Bessel nature of the surface shapes motivates us to investigate, whether the functionality of a liquid lens can be extended to convert a tunable spherical lens into a tunable asphere. In this paper we will confirm the results of our previously published model with a second interferometric approach and investigate to what extend it is possible to create aspheric shapes on the liquid lens.

II. THEORY

Surface vibrations on a LL can be described as a Bessel-function of first type and zeroth order J_0 for sinusoidal actuation.[11,18,21] The Bessel-functions of first type and zeroth order form a complete set of orthogonal basis functions in polar coordinates. This indicates, that for sufficiently large times after switching on the actuator basically any type of surface shape can be created by simple superposition of sinusoidal inputs. The surface u for a single oscillation frequency f_0 at time t is[11]

$$u = A(f_0)\cos(2\pi f_0 t) J_0\left(\frac{2\pi f_0}{c} r\right) \tag{1}$$

where c is the capillary speed of waves, A is the amplitude, and r is the radial coordinate. A desired surface function for $t = 0$ can be expressed as a superposition of such surface functions for different amplitudes $A(f)$ and frequencies f.

$$u(r \le R, t = 0) = \int_0^\infty A(f) J_0\left(\frac{2\pi f}{c} r\right) \mathrm{d}f \tag{2}$$

The surface shape is chosen to be zero for all values outside the lens radius R: $u(r > R) = 0$. To get a specific surface shape $u(r, t = 0)$ the exact time dependent actuation signal can be calculated using two basis transforms. First a Hankel transform to calculate the amplitude spectrum of the surface function and second an inverse Fourier transform to obtain the time dependent actuation signal for the LL. The Hankel transform is defined as:[22]

$$\mathscr{H}_0[u(r)](k) = \int_0^\infty u(r) J_0(kr) r \, \mathrm{d}r \tag{3}$$

with k being the scaling factor along the r-axis. Applying the Hankel transform on Eq. (2) yields:

$$\mathscr{H}_0[u(r, t = 0)] = \frac{c}{2\pi f} A(f) \tag{4}$$

using the orthogonality property of the Bessel function[23] $\int_0^\infty J_n(k'r) J_n(kr) r \, \mathrm{d}r = \delta(k' - k)/k$ and $k = 2\pi f/c$. The linear dispersion is only valid for small waves and frequencies and must be replaced with a more complicated one in more exact fluid models.[21]

The electrowetting[24] boundary condition determines the contact angle deviation θ of the liquid surface at the lens radius R

$$\left.\frac{\partial u(r \le R, t)}{\partial r}\right|_{r=R} = -\tan\theta. \tag{5}$$

The voltage actuation signal $U(t)$ is proportional to $U(t) \sim \tan(\theta)$ for small angles. Applying the boundary condition to the model and evaluating it for the derived amplitude spectrum $A(f)$ (Eq. (4)) for a desired surface $u(t = 0)$ yields the voltage spectrum

$$\hat{U}(f) \sim \left(\frac{2\pi f}{c}\right)^2 J_1\left(\frac{2\pi f}{c} R\right) \mathscr{H}_0[u]. \tag{6}$$

The time-dependent actuation signal is given by the inverse Fourier transform:

$$U(t) = \int_{-\infty}^{\infty} \hat{U}(f) \exp(2i\pi f t) \, \mathrm{d}f \tag{7}$$

The hereby obtained actuation signal $U(t)$ can now be used to stimulate oscillations on the liquid lens that add up to the desired surface function u at $t = 0$. The obtained signal is infinitely long but in

fact for finite lens sizes only a short pulse holding non-zero information. The pulse can be repeated continuously to recreate the desired surface function at video rate.

III. IMPLEMENTATION

The presented transforms were implemented in Matlab using its discrete fast Fourier transform (FFT) and the quasi-discrete Hankel transform.[25,26] The Hankel transform is applied on an array containing the desired surface coordinates u at $t = 0$ to obtain the spatial spectrum $H[u(r, t = 0)](k)$. The spatial spectrum is transformed into the temporal voltage spectrum $\hat{U}(f)$ using Eq. (6). The resulting voltage signal $U(t)$ is obtained by the inverse FFT. The calculation time to obtain the voltage signal is 24-30 ms on a standard desktop machine (Intel Core i5-3470) independent of the complexity of the desired surface input. The example of the first resonant Bessel mode $u(r \leq R, t = 0) = J_0(j_{1,1}r/R)$ with $j_{1,1}$ being the first root of the Bessel function of first type and first order is used to illustrate the intermediate steps of the algorithm (FIG. 1). The Hankel transform converts a Bessel function into a sharp peak at the resonance frequency. The peak width and the side modes are a direct consequence of the discrete transforms. They enforce resulting signals to be of limited length and resolution. In other words, the finite radius R of the lens determines the length of the determined actuation signal. The determined signal is therefore always a pulse, even if a continuous signal could be used to achieve the same result.

To check the validity of the Hankel-transform method, its result is compared to the analytic actuation signal for the second resonant Bessel mode $u(r \leq R, t = 0) = J_0(j_{1,2}r/R)$ in FIG. 2. Within the first half of the pulse, both methods create the identical signals. The second half of the pulse is symmetric and destroys the surface shape to restore a flat surface. At $t = \pm 20.4$ ms the pulse ends. The pulse length resembles the traveling time of a wave on the lens from one side to the opposite side and is given by the ratio of the radius R of the lens and the speed of waves on the LL surface c.

The applicability of the method will be demonstrated experimentally with four different examples: The trivial case of creating a Bessel shape on the LL surface, a Zernike polynomial to address

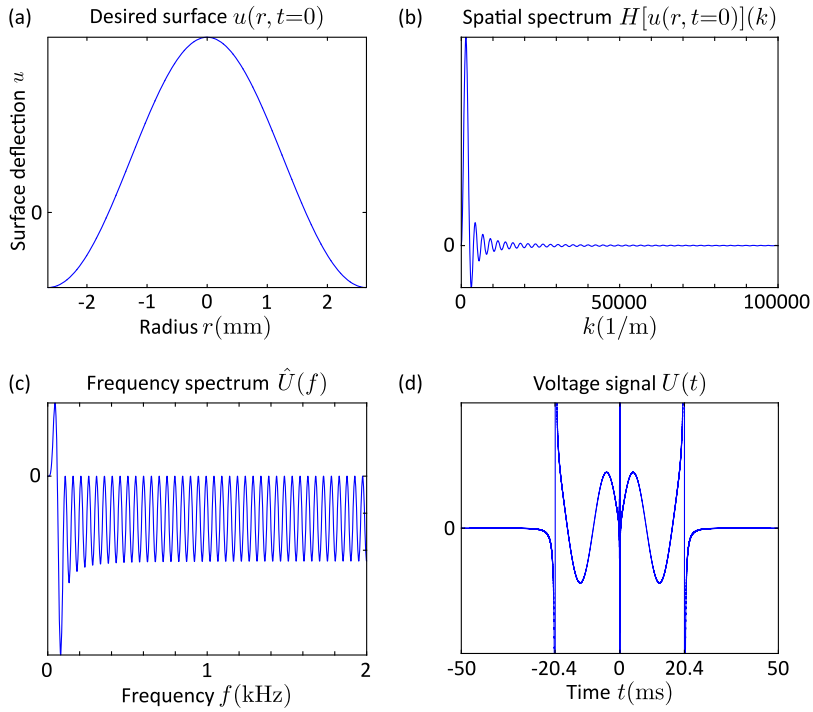

FIG. 1. Illustration of the working principle of the Hankel transform algorithm. The desired surface shape u (here: first Bessel mode) is taken as an input function (a) and converted into its Bessel components H_0 (b). The frequency spectrum of the actuation voltage $\hat{U}(f)$ is displayed in (c) and then Fourier transformed to obtain the voltage actuation signal $U(t)$ (d).

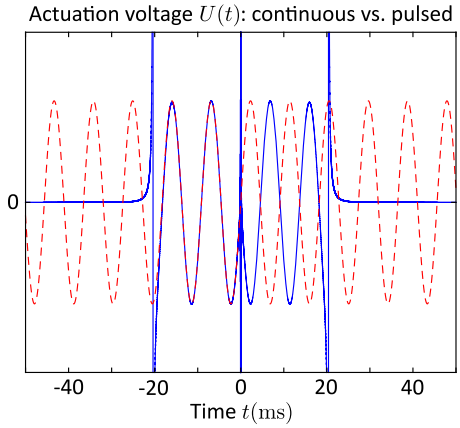

FIG. 2. Comparison of the actuation signal for the second resonant Bessel mode on the LL for an infinitely extended lens using the analytic model (red) and a finite lens radius using the proposed Hankel transform method (blue).

spherical aberrations, a conical surface to create an axicon and a top hat structure to show the limitations of the model.

IV. EXPERIMENT

The used LL is a Varioptic Arctic 39N0 by Corning.[27] During standard operation the optical power ranges from -5 m^{-1} to 15 m^{-1} for voltages from 39 V to 58 V. A flat surface can be obtained for ± 45 V. The maximum voltage range is 24 - 70 V. The lens makes use of AC electrowetting, therefore all input voltages are modulated with a square wave at 1136 Hz. At 632.8 nm, the refractive indices of the two used liquids are $n_1 = 1.3846$ and $n_2 = 1.4921$. The response time between two extreme foci is 20 ms and the root-mean-squared (RMS) wavefront error is $\mathrm{WFE}_{rms} = 50$ nm (i.e. $(n_2 - n_1) \times \mathrm{WFE}_{rms} = 0.5$ μm RMS surface error). The speed of capillary waves has been found to be $c = 26$ cm/s.[11] The measurement temperature is $T = 25°$C. The radius of a flat LL interface is $R = 2.65$ mm.

A HeNe laser beam is collimated and sent through a Mach-Zehnder interferometer (FIG. 3). The light passing through the liquid lens interferes with the reference and is measured with a camera. A lens is used behind the Mach-Zehnder interferometer to image the optical phase shift introduced by the LL surface onto the camera. The camera is a SVS-VISTEK eco424MVGE with an adjustable frame rate (1 - 124 Hz) and integration time (3 μs - 1 s). All videos are made using an external trigger to synchronize the camera to the LL surface movement. The videos are in consequence not showing a high-speed image of a single lens surface oscillation but are recorded over many oscillation periods. The calculated voltage signal is sent via a NI-9263 D/A converter from the computer to a voltage amplifier (8×) and then applied to the LL electrodes.

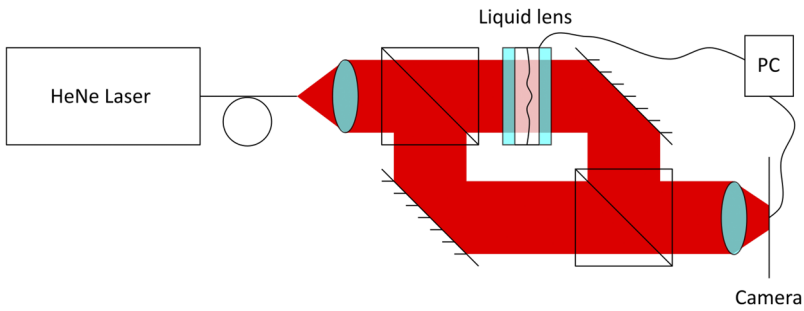

FIG. 3. The liquid lens surface is measured in a Mach-Zehnder interferometer. The phase change due to the liquid lens is imaged onto the camera with an additional lens.

The interferogram is analyzed in Matlab using standard FFT techniques[28] and 2D phase unwrapping.[29]

V. RESULTS

The presence of Bessel shaped modes as predicted by the previously published analytical model can be additionally confirmed with the interferometric surface measurement. A cosine voltage with an amplitude of 1.6 V and a frequency of 59 Hz is applied to the liquid lens to reproduce the first resonant Bessel mode.[11] Figure 4(a) (Multimedia view) shows the measured surface profile for maximum deflection along the y-axis of the camera sensor. The measurement surface shape agrees to the model (compare Eq. (1)). The RMS wavefront error WFE_{rms} = 0.02 μm is smaller than the one given by the LL manufacturer. The RMS wavefront error of 0.01 − 0.02 μm can be observed in all measurements (even without the LL) and is therefore associated with the Mach-Zehnder interferometer. The movement of the liquid lens surface is not entirely symmetrical, when applying a cosine voltage as can be seen in the video. The behavior of the surface changes slightly with the polarity. This asymmetry has been described recently[30] and can be explained by the theory of charge restraint. Negative ions are restrained more easily by the dielectric during the oscillation and therefore prevent the formation of a flat surface in half of the cases. The video of the surface oscillation is taken with time steps of 292 μs/frame and the exposure time is 80 μs.

The same surface shape can be created using the proposed algorithm as displayed in FIG. 4(b) (Multimedia view). A pulse is calculated for the first Bessel mode on the liquid lens as shown in FIG. 1. The pulse is repeated with a frequency of 10 Hz. The video shows the pulse in time steps of 62.5 μs/frame and the exposure time is 20 μs. The Bessel function is created with the same quality (WFE_{rms} = 14 nm) as with the continuous actuation voltage. However, the surface profile looks very different at all other times than $t = 0$.

Creating a Zernike function like deformation that can be added to the spherical surface of the LL is an application of the technique. The primary spherical aberration Z_4^0 can be created in the same way as the Bessel surface shapes. Figure 5 illustrates the result of the algorithm and shows the created surface and the surface profile. The peak to valley deflection of the surface is 3 μm, which resembles an optical phase difference of π. The change in phase can be chosen to be smaller than 2π as well as larger than the wavelength. The smallest phase change tested successfully is 0.16π. The absolute deviation from the desired surface is similar to the previous examples (WFE_{rms} = 0.02 μm) but is relatively larger due to the choice of a smaller surface deflection.

Surface shapes with higher spatial frequency content are more difficult to create. An axicon is for example still possible with good accuracy using the linear dispersion model, but a top hat structure cannot be created. Figure 6(a) shows the measured surface shape of an axicon. While the slopes of

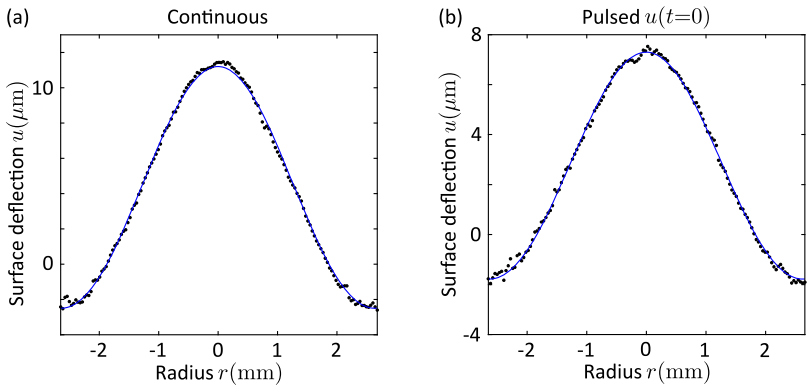

FIG. 4. The Bessel function created in two different ways: (a) by a continuous 59 Hz cosine actuation signal and (b) by a pulsed signal as shown in FIG. 1 (black dots). The theoretical prediction is plotted in blue. Multimedia views: https://doi.org/10.1063/1.5063994.1; https://doi.org/10.1063/1.5063994.2

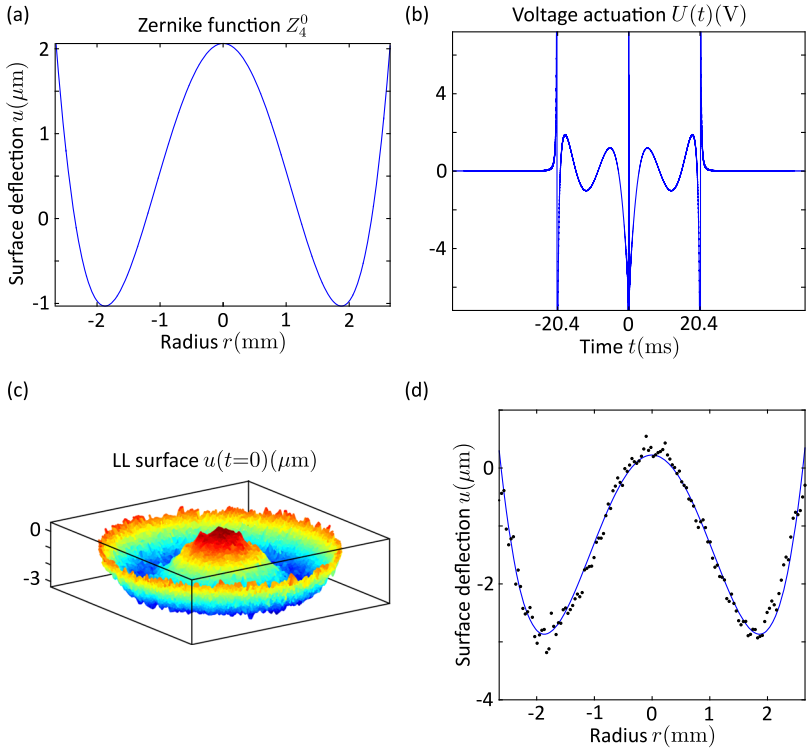

FIG. 5. The primary spherical aberration (a) is transformed into a voltage actuation signal (b). The surface measurement is displayed (c) and a surface profile is shown (d).

the axicon are nicely mimicked (WFE_{rms} = 0.02 μm), the tip of the axicon appears slightly rounded and loses its sharpness for higher amplitude signals.

The top hat structure is displayed in FIG. 6(b). The slopes of the top hat are too steep to be fully described by the simple membrane-based model. The measured surface slope is 6 μm/mm which equals an optical path length difference of one optical wavelength per millimeter for a HeNe laser. The slope limitation is not constant over the lens diameter but it is proportional to the envelope of the Bessel functions ($\partial u/\partial r \sim \sqrt{2/(\pi r)}$ for large radii). Large slopes close to the center of the lens need high actuation frequencies. Everywhere else, larger slopes require larger actuation voltages in the input signal and thus are affected more by non-linearities. A description of the surface vibration, that takes account of the non-linear dispersion of capillary waves, the exact lens geometry, and the viscosity is expected to improve the creation of high-frequency surface shapes.

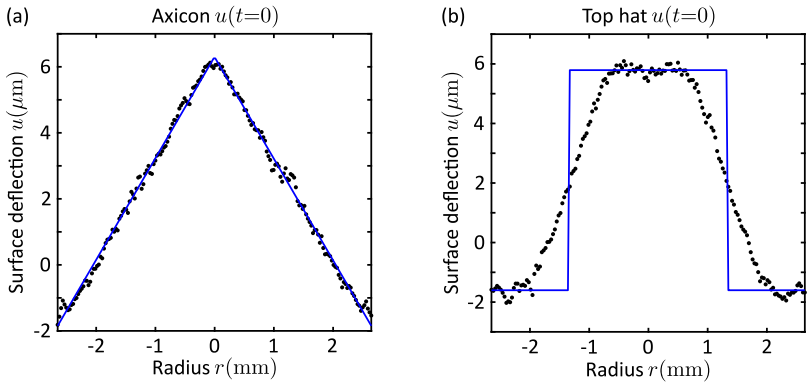

FIG. 6. A pulsed signal is used to design a specific surface shape (blue) and measured interferometrically (black dots) for (a) an axicon and (b) a top hat.

The presented results are highly repeatable. A difference in the resulting wavefront exceeding the 50 nm RMS wavefront error has neither been found, when measuring the surface shape of the LL for a specific actuation signal over several days in a row, nor when repeating the same experiment after 109 days.

The radius of the LL is directly responsible for the calculated pulse lengths and therefore imposes a limit on the maximum repetition rate of the desired liquid lens surfaces. To increase the repetition rate, the pulse can be shortened to half its length by setting the actuation voltage to zero for $t > 0$.

VI. CONCLUSIONS

A new way to create aspheric surfaces on a liquid lens has been demonstrated. The proposed Hankel transform method can calculate the voltage actuation signals to generate any surface shape temporarily on the LL. However, friction and the viscosity of the liquid limit the applicability of the undamped model to surface deviations in the range of a few optical path lengths. The underlying simplification of a linear surface wave dispersion further limits the shapes to low spatial frequencies. The creation of a Bessel function, the primary spherical aberration Zernike polynomial, and an axicon has been demonstrated successfully. Creating a top hat structure however failed due to the simplicity of the underlying liquid model but could be improved by considering a more thorough liquid dispersion model.

ACKNOWLEDGMENTS

This work is funded through the Spectr@phone project (IPD 12017) of the IOP Photonic Devices program of RVO.

[1] B. Berge and J. Peseux, Eur. Phys. J. E **3**, 159 (2000).
[2] S. Kuiper and B. H. W. Hendriks, Appl. Phys. Lett. **85**, 1128 (2004).
[3] G. S. Jung, J. S. Lee, and Y. H. Won, Proc. SPIE **10545**, 1054516 (2018).
[4] F. Zhang, Y. Yao, X. Qu, T. Zhang, and B. Pei, Opt. Laser Technol. **88**, 198 (2017).
[5] Y. Shimizu, D. Koyama, M. Fukui, A. Emoto, K. Nakamura, and M. Matsukawa, Appl. Phys. Lett. **112**, 161104 (2018).
[6] A. Y. Malyuk and N. A. Ivanova, Appl. Phys. Lett. **112**, 103701 (2018).
[7] K. Mishra, C. Murade, B. Carreel, I. Roghair, J. M. Oh, G. Manukyan, D. van den Ende, and F. Mugele, Sci. Rep. **4**, 6378 (2014).
[8] K. Mishra and F. Mugele, Opt. Express **24**, 14672 (2016).
[9] I. S. Park, Y. Park, S. H. Oh, J. W. Yang, and S. K. Chung, Sens. Actuators, A **273**, 317 (2018).
[10] D. Kopp, T. Brender, and H. Zappe, Appl. Opt. **56**, 3758 (2017).
[11] M. Strauch, Y. Shao, F. Bociort, and H. P. Urbach, Appl. Phys. Lett. **111**, 171106 (2017).
[12] D. R. Schipf and W.-C. Wang, Proc. SPIE **10559**, 1055908 (2018).
[13] Lord Rayleigh, Proc. Roy. Soc. London **29**, 71 (1879).
[14] J. B. Bostwick and P. H. Steen, Phys. Fluids **21**, 032108 (2009).
[15] C. A. Miller and L. E. Scriven, J. Fluid Mech. **32**, 417 (1968).
[16] A. Prosperetti, J. Fluid Mech. **100**, 333 (1980).
[17] O. A. Basaran, J. Fluid Mech. **241**, 169 (1992).
[18] L. D. Landau and E. M. Lifshitz, *Fluid Mechanics*, 2nd ed., Course of Theoretical physics, Vol. 6 (Butterworth-Heinemann, London, 2003).
[19] A. Frohn and N. Roth, *Dynamics of Droplets*, edited by R. J. Adrian, M. Gharib, W. Merzkirch, J. H. Rockwell, and D. Whitelaw (Springer, Berlin, 2000).
[20] L. Wang and M. Ishikawa, Proc. SPIE **10544**, 1054419 (2018).
[21] R. A. Ibrahim, *Liquid Sloshing Dynamics: Theory and Applications* (Cambridge University Press, Cambridge, 2005).
[22] L. Debnath and D. Bhatta, *Integral Transforms and Their Applications*, 3rd ed. (CRC Press, Boca Raton, 2015).
[23] K. B. M. Nambudiripad, *Bessel Functions* (Alpha Science International, Oxford, 2013).
[24] F. Mugele and J.-C. Baret, J. Phys.: Condens. Matter **17**, R705 (2005).
[25] A. E. Siegman, Opt. Lett. **1**, 13 (1977).
[26] M. Guizar-Sicairos and J. C. Gutiérrez-Vega, J. Opt. Soc. Am. A **21**, 53 (2004).
[27] "Corning® Varioptic® Lenses | Driver for Adjustable Lens | Corning," Corning Incorporated, Retrieved on 2018-5-20, http://www.corning.com/worldwide/en/innovation/corning-emerging-innovations/corning-varioptic-lenses.html.
[28] M. Takeda, H. Ina, and S. Kobayashi, J. Opt. Soc. Am. **72**, 156 (1982).
[29] D. C. Ghiglia and M. D. Pritt, *Two-Dimensional Phase Unwrapping: Theory, Algorithms, and Software* (John Wiley & Sons, New York, 1998).
[30] X. Na, Z. Ning, and X. Rong-Qing, Jpn. J. Appl. Phys. **57**, 052201 (2018).